Measurement of the electrical resistivity of a dense strongly coupled plasma

J. F. Benage, Jr., W. R. Shanahan, E. G. Sherwood, L. A. Jones, and R. J. Trainor
Los Alamos National Laboratory, Los Alamos, New Mexico 87545
(Received 2 August 1993)

We present measurements of the electrical resistivity of a dense strongly coupled plasma. This plasma is created in a comprehensively diagnosed capillary discharge that produces uniform well-characterized dense plasmas. Data for polyurethane at densities $\rho=0.01\rho_0$, where $\rho_0=1.265$ g/cm^3, and temperatures in the 25–30 eV range are compared with several dense plasma theories, and show a significant disagreement. These results are of importance for the modeling of pulsed power experiments and the understanding of transport processes in many astrophysical plasmas.

PACS number(s): 52.25.Fi

I. INTRODUCTION

As plasmas become more dense, the Coulomb interaction between particles increases due to their closer average distance. In ideal plasma theory, this interaction is assumed to be small. When the Coulomb potential energy becomes comparable to the thermal energies of the plasma particles, the assumption is no longer valid and the fundamental description of the plasma changes.

There are two dimensionless expansion parameters used to describe the magnitude of the particle-particle interaction. The plasma parameter, $g=1/n_e\lambda_d^3$, where n_e is the electron density and λ_d is the Debye length, is used for low density plasmas. The equations generally used to describe the properties of a plasma are obtained by reducing the exact many body equations to single particle equations. These equations are valid only when $g \ll 1$, since the magnitudes of the neglected part of the many body equations are of order g. When g becomes of order one, the Debye length no longer has physical meaning and this standard approach for describing plasma properties is no longer appropriate. In this case, we generally use the parameter Γ, which is defined as the ratio of the average potential energy between particles to their kinetic energy. This is written for ions as

$$\Gamma=\frac{Z^2e^2}{akT}\ , \tag{1}$$

where $a=(3/4\pi n)^{1/3}$, Z is the average ionization level, and n is the ion density. Γ is related to g by $\Gamma=Z^{5/3}g^{2/3}/3$. When Γ is of order one or greater, the plasma is said to be strongly coupled. Under these conditions, new theoretical descriptions are required to describe the properties of the plasma.

Examples of strongly coupled plasmas are the interiors of white dwarfs and brown dwarfs, laser produced plasmas, high-power electrical fuses, plasma opening switches, laser-cooled plasmas, capillary discharges, and other pulsed power produced plasmas. In general, anytime dense material is rapidly heated so that it reaches plasma conditions before it can expand significantly, it will temporarily reside in the strongly coupled regime.

Theoretical treatments of strongly coupled plasmas are based on a variety of approaches. Many theories use a dielectric or classical approach [1–6] to describe the equation of state (EOS) and various transport properties. Others use various quantum mechanical approaches [7–9]. Still others use computer simulations to describe the properties of the plasma [10,11]. Many of these theories are able to match data where data are available. The problem is that there is such a paucity of data, especially for highly ionized systems, that for the most part these theories have not been rigorously tested. Early experiments studied alkali metals [12] and inert gases [13]. More recent experiments have focused on improving techniques for producing and diagnosing these plasmas. These include reflectivity measurements from laser produced plasmas [14,15], ion traps to measure ion structure [16], discharges for measuring resistivity [17,18], and opacity measurements using laser produced plasmas [19]. There is also a body of work from the former Soviet Union that has been reviewed by Fortov and Iakubov [20].

In this paper we describe results of electrical resistivity measurements of a dense strongly coupled polyurethane plasma produced in a capillary discharge. The technique produces uniform, relatively long-lived plasmas, which are amenable to comprehensive diagnosis and modeling. A description of preliminary experiments of this type has been given by Shepherd, Kania, and Jones [18]. Conditions achieved for polyurethane are electron densities near 5×10^{21} cm^{-3} and temperatures of 25–30 eV corresponding to $\Gamma\approx0.6$–0.8. Transport properties in this parameter regime have not previously been investigated.

II. DESCRIPTION OF THE EXPERIMENT

The plasma is produced in a capillary discharge, consisting of an insulator with a small diameter hole (typically 20 μm) down the axis placed between two electrodes. A rapidly rising high voltage is applied across this hole and current is initiated.

Once the discharge has been initiated, the plasma produced from the wall material will pinch, causing the current to be pulled away from the wall to further heat the plasma as it pinches. Very quickly the temperature of the plasma rises enough that radiation begins to ionize material on the wall. Once this begins, the current couples to the wall and the density of the plasma will in-

crease as material is ablated off. This process continues until an equilibrium situation is produced consisting of the plasma density and temperature remaining nearly constant with the power input being balanced by new material being ablated into the plasma, losses out the end of the capillary, and other radiative losses. The time for equilibrium to be achieved is just the time it takes for the plasma pressure in the capillary to exceed the magnetic pressure. This can be determined by equating the pressure produced in the discharge to the magnetic pressure. We can write the thermal pressure assuming no losses as

$$P_T=(Z+1)nkT = \frac{(Z+1)\rho N_A kT}{A} = \frac{(Z+1)N_A}{A}\int_0^t \frac{I^2\eta dt}{\pi^2 r^4 \bar{C}_v} , \quad (2)$$

where $\bar{C}_v$ is the average specific heat, ρ is the mass density, A is the average atomic mass number, N_A is Avogadro's number, I is the current, η is the resistivity, r is the radius of the capillary, and T is the temperature of the plasma. The magnetic pressure is given by

$$P_B=\frac{\mu_0 I^2}{8\pi^2 r^2} . \quad (3)$$

Assuming the current I is proportional to t (which approximately describes the discharges in this experiment) and equating these pressures we can solve for t to get

$$t=\frac{3\mu_0 \bar{C}_v r^2 A}{8(Z+1)N_A \eta} . \quad (4)$$

For times greater than t, the capillary discharge will be in equilibrium.

The parameters of the plasma under these conditions depend on the power levels applied to the discharge. For this experiment, we use a Marx bank charged to an energy of 27 kJ that provides a peak current of 240 kA in a near-sinusoidal wave form with a $\frac{1}{4}$ cycle time of 220 ns. The initial I dot of this current is 1.6×10^{12} A/s. The capillary used in the experiments reported here is made of polyurethane, which has a chemical composition by weight of 62% carbon, 9% hydrogen, 5% nitrogen, 24% oxygen, and a few trace elements. The initial capillary diameter is 20 μm. Using Eq. (4) for our conditions, we find that the plasma reaches equilibrium condition in ≈ 10 ns. This number is consistent with numerical calculations discussed later, which show that by 3–4 ns, the plasma has become uniform in density and temperature and fills the entire capillary. Because of the high power deposited in the discharge, the pressure balance is not maintained. Soon the pressure produced in the plasma becomes much greater than the magnetic pressure and is enough to produce a shock wave in the polyurethane. The plasma acts as a piston, pushing material radially outward and causing the radius of the discharge to increase. The plasma parameters are determined by the balance between the energy input and the energy required to heat the new material being ablated, the work done by the plasma, and radiative energy lost to the wall. The energy lost out the end by plasma flow is not important because the length to diameter ratio l/d for the capillary is so large ($\sim 10^3$) and the discharge occurs for such a short time that very little material can leave. The discharge consists of three regions: a region of the current carrying channel where the material is in the plasma state; a region where the polyurethane has been compressed by the shock wave; and a region where the polyurethane has not been disturbed. This system is similar in principle to a laser deflagration preceded by a shock wave [21].

The electrical resistivity of the plasma is obtained from several measurements: the current through the plasma, the voltage drop across the plasma, and the radius of the plasma. The pressure and temperature of the plasma are also measured, and the plasma density is then calculated from energy balance, using the measured input power and plausible models for the EOS. A schematic of the experimental setup is shown in Fig. 1. Between the anode and cathode is a cylindrical block of polyurethane with a 20 μm diameter capillary down the 2 cm long axis. Several diagnostics are shown in this diagram: a Rogowski coil to measure the current, a capacitive voltage probe, a microchannel-plate (mcp) framing camera that records four images of the propagating shock in the polyurethane, and a pinhole x-ray framing camera that looks through a hole in the anode to image the discharge and measure the intensity of radiation emitted.

The voltage measured by the capacitive probe is the entire voltage drop across the plasma and has two components, a resistive component and inductive component. To correct for the inductive component, shots are fired into a shorted load with the same geometry except the plasma region is replaced by a metal rod of radius 0.5 cm. We can then measure the total inductance of the load and correct this for the difference in radius between the plasma and the short. The current is measured utilizing a Rogowski coil which has been calibrated with a Pearson self-integrating Rogowski.

The position of the radially expanding shock is measured by imaging the capillary on four different mcp's. Each mcp is gated separately at appropriate times giving four independent snapshots of the diameter of the shocked region of polyurethane and thus the shock speed.

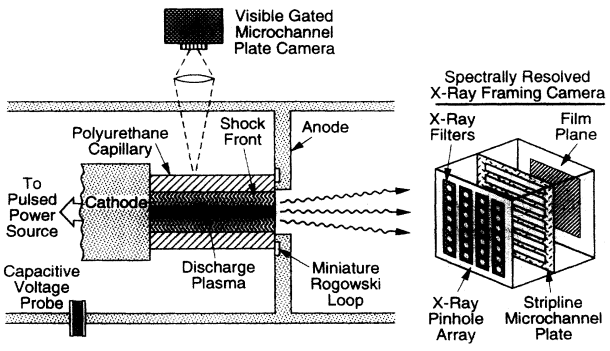

FIG. 1. A schematic of the experimental setup to measure the electrical resistivity in the plasma.

The measured speed of the shock gives the pressure behind the shock in the polyurethane, since the EOS of shocked polyurethane is known in this regime [22]. The shock pressure and the plasma pressure are closely related, differing primarily by the shock pressure decay associated with the divergent geometry. This decay is calculated with a hydrocode in a reliable manner. Thus, our measurement of shock speed produces a relatively accurate inference of the plasma pressure.

The x-ray pinhole framing camera has proved to be extremely useful for an accurate description of the discharge and determination of the plasma parameters. This device consists of a stripline mcp whose operation is described fully by Young, Stewart, Woodworth, and Bailey [23]. The mcp contains seven gold striplines as photocathodes which can be separately pulsed. The plasma is imaged onto each of these seven striplines using a pinhole array consisting of four columns of seven pinholes each. In front of each column is an x-ray filter to restrict the spectral range which is imaged by that column. Consequently, this device can measure the x-ray emission from the plasma in four different spectral regions at seven different times in two dimensions. We use this information to determine the diameter of the current carrying channel and the temperature of the plasma.

The temperature of the plasma is determined using the two-filter technique, which has the advantage of not requiring an absolute measure of the intensity. In this technique the plasma is assumed to be a blackbody radiator. The temperature is determined by comparing the relative intensity in one spectral region to that in another. This works quite well in that the ratio can be sensitive to temperature if the spectral regions are properly chosen. In this experiment we have chosen four filter materials: aluminum, which transmits in the energy range of 30–70 eV; silicon, which transmits from 70–100 eV; boron, which transmits from 120–190 eV; and carbon, which transmits from 200–290 eV. The critical assumption in this measurement is that the plasma is a blackbody radiator. Because of the densities and temperatures involved, we expect the plasma to be optically thick in these energy regions. As with all plasmas though, one must take into consideration the boundary effects on the radiation emitted. We shall see when looking at the data that this is important in our experiments as well.

III. DESCRIPTION OF THE PLASMA MODEL

The modeling of the capillary discharge has proved invaluable in the interpretation of the experiment and has led to more sophisticated and accurate diagnostics than previously used. We have used two types of models. The more sophisticated of these is a one-dimensional (1D) magnetohydrodynamic (MHD) computer code called RAVEN. This code is based on methods described elsewhere [24]. RAVEN is a complete resistive MHD code with thermal conductivity, radiation transport, and access to the SESAME library of resistivity and equation of state tables. Calculations using RAVEN were the first to indicate that the dynamics of the capillary discharge were different from that previously reported [18]. This discovery led to the development of a new diagnostic, the pinhole x-ray framing camera, for measuring the properties of the capillary discharge [25]. The results from this diagnostic verified the RAVEN predictions and have led to new results for the experiment.

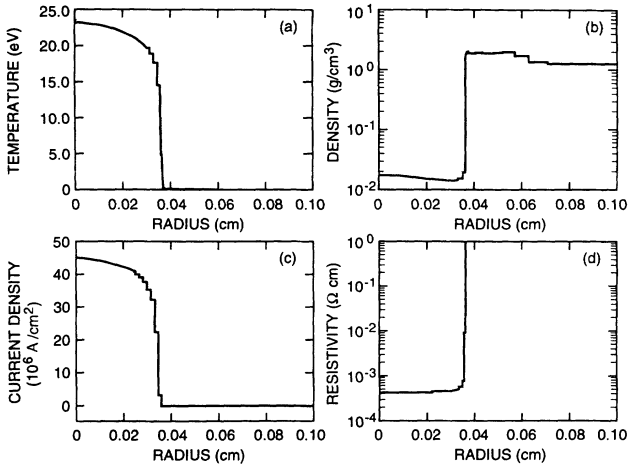

FIG. 2. Predictions of the RAVEN code: (a) Radial profile of plasma temperature at a time 100 ns into the discharge; (b) radial profile of the mass density at a time 100 ns into the discharge; (c) radial profile of the current density 100 ns into the discharge; and (d) radial profile of the electrical resistivity 100 ns into the discharge.

Some examples of the calculations done by RAVEN are shown in Fig. 2. These calculations use the current from the experiment and initiate the breakdown by starting the first zone at 0.5 eV. These figures show radial profiles for the current distribution, resistivity, temperature, and density at a time of 100 ns into the discharge. The density curve is useful in that it graphically illustrates the three regions of the discharge, i.e., the low density plasma region, the high density shocked region, and the region of undisturbed polyurethane. All four traces illustrate the uniformity of the plasma. A high level of uniformity in the current is required for us to determine the resistivity from the measured resistance of the plasma.

Our other model is a 0D model that is described briefly here and more details can be obtained elsewhere [26]. This model uses the conservation of mass, momentum, and energy, assumes the plasma conditions are described by Saha equilibrium, uses the ideal gas law equation of state, and the Hugoniot relations for polyurethane to describe the plasma conditions and dynamics of the discharge. This model assumes the sound speed in the system is infinite so that changes in pressure are communicated throughout the discharge instantaneously. It also assumes that the conditions in each of the regions is uniform. The advantage of this model is that one can make many types of changes to the equation of state and resistivity and to the ablation process to get a better understanding of the discharge. It has provided results close to that from RAVEN.

IV. RESULTS AND ANALYSIS

Figure 3 shows the measured current profile and corrected voltage for the plasma. One can see that as

time increases and the discharge channel increases in size, the resistance drops and the net voltage also drops, even though the current is still rising.

Figure 4 shows the shock radius as a function of time and compares this to both the RAVEN calculation and the prediction from the 0D model. Both models are able to reproduce these data accurately. This radius was thought to be the radius of the discharge in previous experiments [18]. Measurement of the actual plasma radius required using the x-ray pinhole framing camera. The results of those measurements are shown in Fig. 5, where the radius of the emitting region is plotted vs time. Initially, the calculations match the data well but not at later times. A possible reason for this is that the radii we measure may not correspond to the very edge of the plasma. We can see this by looking at Fig. 6, which shows images from the x-ray pinhole framing camera. Here we see three columns of images of the plasma channel, the fourth column is too dim to see. Note that the boron and carbon filtered images are not quite the same size. Since the carbon channel is sensitive to a higher energy band of radiation, the film exposure will be very sensitive to the temperature of the emitting area. Thus if the temperature drops below about 20 eV, the film will not be exposed through the carbon filter. With the boron channel, this effect will occur at a lower temperature because the boron transmits radiation at a lower energy. What we see then is that the radius as measured by the boron channel is larger than the carbon channel because of the slight temperature gradient. The RAVEN calculation shown in Fig. 2(a) predicts that the temperature is fairly uniform across the plasma, but drops rapidly at the wall.

This leads us to expect that the two channels would indicate similar plasma radii; that they differ indicates that the temperature gradient near the wall is not as sharp as predicted. One possible reason that RAVEN may not predict the temperature profile correctly is that the radiation transport in the code is based upon the diffusion approximation, which is correct only for optically thick plasmas where there are no sharp temperature gradients. Since we do not believe that these plasmas are optically thick in the radial direction, we expect this part of the dynamics to be the most suspect. Another explanation is that the EOS used by the code is not correct. This idea was tested using the 0D code with a range of EOS models. The result was that plausible changes in the EOS do not affect the radius of the plasma significantly. We also found that no reasonable changes in the resistivity could reproduce the data. We therefore believe that the temperature profile is not as sharp as the code predicts.

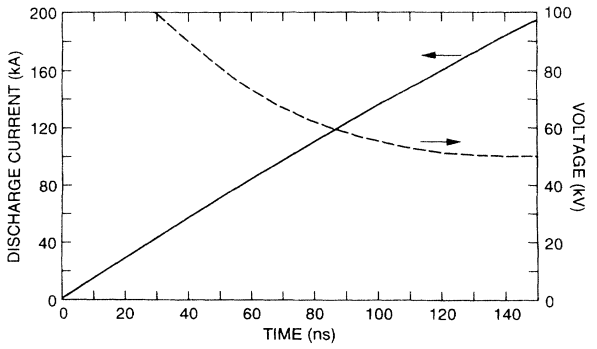

FIG. 3. Measured resistive voltage across the plasma and current through the plasma as a function of time.

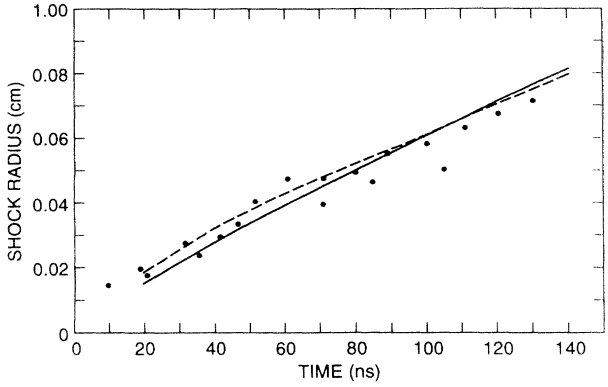

FIG. 4. Radius of the shock front as measured from the visible side-on framing camera. The dotted line is the RAVEN calculations and the solid curve is from the 0D model.

This slight nonuniformity in the temperature profile does not significantly affect our determination of an electrical resistivity, as demonstrated by the following argument. Since the channel radius is small compared to the skin depth for the current, the current density will be proportional to $1/\eta$. Also, since the energy deposited into the plasma is proportional to the integral of ηJ^2, the plasma will be hotter where the current is flowing. In this region of density and temperature, the various theories predict that η is approximately proportional to $1/T$, and therefore the current density will be higher in the regions where the plasma is hot and radiating. This implies that even if the temperature is not constant across the center region, the electrical resistivity determination will not be affected much as long as most of the temperature drop occurs near the wall. Our measurements are consistent with this situation, and we believe that using

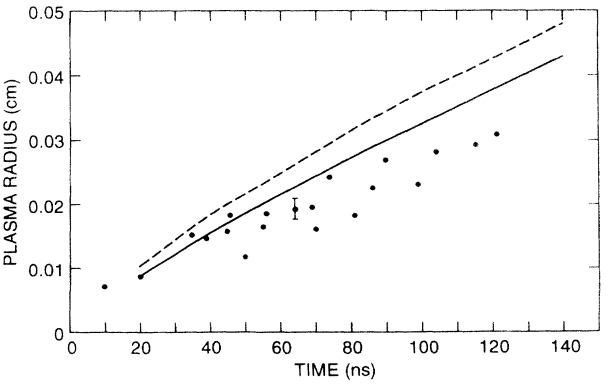

FIG. 5. Radius of the edge of the plasma as measured from the x-ray framing camera using the boron filter. The dotted line is from the RAVEN calculations and the solid line is from the 0D model.

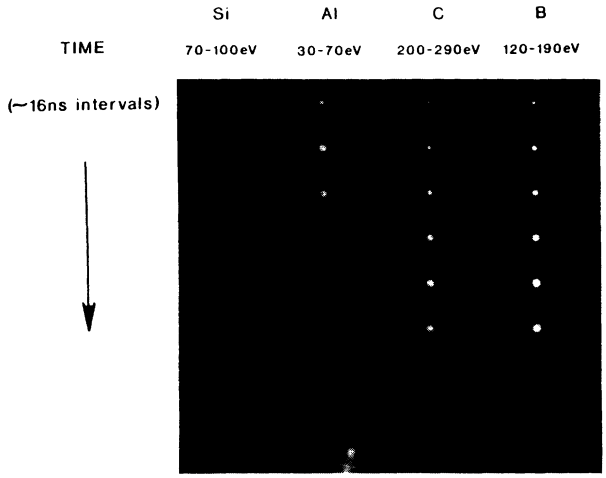

FIG. 6. Image of the end of the discharge using the pinhole x-ray framing camera. Each row is a single time and the time separation between each row is approximately 16 ns. Time goes from top to bottom. The columns each represent a different filter and from left to right these are 1.5 μm silicon, 0.65 μm aluminum, 2 μm paralyne-N, and 0.75 μm boron.

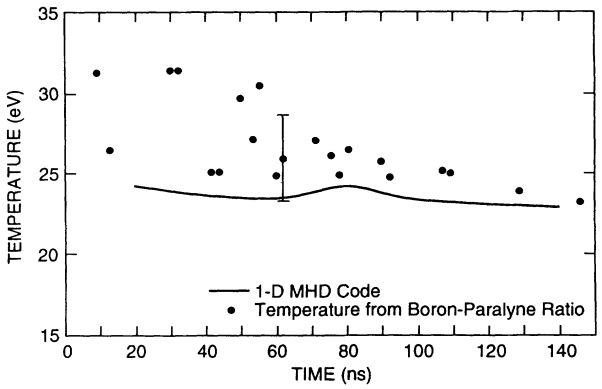

FIG. 7. Temperature determined from the ratio of the x-ray signals in the boron and paralyne-N channels. The solid curve is the temperature in the center of the discharge from the RAVEN calculations.

the edge of the plasma as measured with the boron filter for the plasma radius does not introduce serious errors in the resistivity we determine.

We were not able to measure the edge of the cooler plasma directly as that required using a lower energy filter. The aluminum filtered column was sensitive to a lower energy band but there were different problems encountered with this channel. This problem stems from effects due to plasma blowoff from the plasma surface at the anode. As this plasma cloud gets thicker and cooler, it will eventually become optically thick in the wavelength region of interest. We can see this by looking at the late time frames for the aluminum filtered channel in Fig. 6. For the photon energy transmitted by the aluminum channel, this effect occurs by about 50 ns into the discharge. After this time the images of the aluminum channel see not the plasma but only the blowoff.

The measured plasma temperature, using the ratio of the transmitted intensities from the boron and carbon channels, is shown in Fig. 7. The temperature very quickly rises to near 30 eV and then drops to 25 eV after 120 ns. RAVEN predicts a slightly lower temperature. We believe the discrepancy stems from the fact that RAVEN assumes the plasma is optically thick and therefore may overestimate the amount of radiation produced. This will produce more ablation than would actually occur, thus lowering the calculated temperature. The 0D code can predict the observed temperature if the ablation rate is modified by assuming that only a fraction of the radiated energy from the center region of the plasma reaches the wall and ablates material. This effect of reduced ablation, which has been called the vapor shielding effect, has been seen elsewhere [27] and verified experimentally. The fraction needed to reproduce the temperature is 20% of the radiated energy, which is nearly the same as that found in Ref. [27].

To compare the measured electrical resistivity to theory, we must know the ionization level and the density of the plasma. We use calculations from the 0D and 1D models to obtain these quantities, since direct measurement is difficult. These calculations give the temperature, pressure, density, and ionization level of the plasma. The calculations of pressure and temperature can be compared directly with data, while the ionization level and density are determined using the measured energy deposition and a plausible EOS model. In the case of the RAVEN calculations, we initially used a modified ideal gas EOS in Saha equilibrium, which does not treat particle correlations that may be important for strong coupling. We therefore incorporated correlation effects into the 0D MHD model using EOS models that probably overestimate the correlation energy and predicted a higher density than the RAVEN calculations by about a factor of 2. However, the temperature predicted by the RAVEN calculations is slightly lower than measured, which would tend to push the density slightly lower if the calculated value were made to agree. The net result is that the uncertainty in the density of the plasma is at most a factor of 2 in either direction. The uncertainty in the ionization level of the plasma is very low, $\sim 10\%$. This is because at these temperatures, the hydrogen will be nearly fully stripped and the carbon will mostly be in the heliumlike state and this will be rather insensitive to the density in this range. These uncertainties have only a small effect on comparison to theories, as all the theories predict a very weak density dependence of electrical resistivity in the measured temperature range. For example, the Spitzer theory depends on density only through a logarithmic term. The net result is that there is an uncertainty of 10–20 % in the resistivity obtained from theory due to the uncertainties in ionization level and density.

The electrical resistivity as a function of temperature is plotted in Fig. 8, where the error bars in the temperature are from the measurements and the fit to the temperature vs time data and the error bars in resistivity are due to just the error in making the measurements. These are

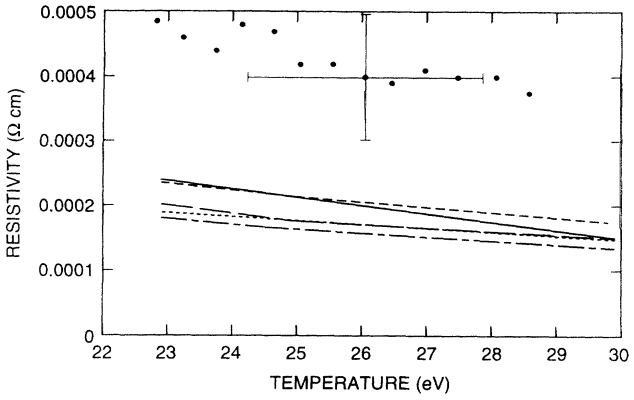

FIG. 8. Electrical resistivity as a function of temperature in comparison with several theories. The bullets denote experimental measurements; the medium dashes denote Ref. [3]; the short dashes denote Spitzer; the straight line denotes Ref. [8]; the long dashes denote Ref. [2]; the long dash, short dash denotes Ref. [4].

compared against several theories, most of which agree with each other in this parameter regime. None of the theories agree with the data, which are a factor of 2 higher than these predictions. A possible explanation can be found in the recent work by Ichimaru [28], who has shown that in this parameter regime of nondegenerate plasma with $\Gamma \cong 1$, the electron-ion structure factor plays a critical role in transport processes. He also points out that electrons in Rydberglike states can scatter conduction electrons and therefore cause an increase in resistivity. Another possible reason for the discrepancy may be that the theories have not included all the ion species in polyurethane. However, the calculations that do include carbon and hydrogen such as those of Rinker and Dwarma-Wardana do not show significant differences. It may be that these theories are not able to treat systems with more than one ion species.

V. CONCLUSION

We have completed an experiment measuring the electrical resistivity of a dense strongly coupled plasma. We produced these plasmas in a capillary discharge that we extensively modeled and diagnosed. This plasma had a computed electron density of 5×10^{21} cm^{-3} and a measured temperature of 25–30 eV, corresponding to a coupling parameter of $\Gamma=0.6$–0.8 with average Z of 2.3 assuming Saha equilibrium. The results of this experiment indicate that most theories do not accurately predict the resistivity in this parameter regime. More work must be done in this area to cover other parameter regions and produce more definitive answers. We conclude that it would be useful to do experiments on single elements to reduce the complexity of theoretical calculations. Work on materials such as aluminum and copper is planned.

ACKNOWLEDGMENTS

We would like to take this opportunity to acknowledge many useful discussions with J. V. Parker, G. A. Rinker, and many others. We would also like to express our appreciation for the valuable technical assistance provided by D. P. Nothwang and S. E. Linzey in carrying out the experiments. This work was performed under the auspices of the U.S. DOE.

[1] M. Baus, J. P. Hansen, and L. Sjorgren, Phys. Lett. **82A**, 180 (1981).
[2] D. B. Boercker, F. J. Rogers, and H. E. Dewitt, Phys. Rev. A **25**, 1623 (1982).
[3] R. Cauble and W. Rozmus, J. Plasma Phys. **37**, 405 (1987).
[4] S. Ichimaru, S. Mitake, S. Tanaka, and X-Z. Yan, Phys. Rev. A **32**, 1768 (1985).
[5] W. D. Kraeft, J. Blumlein, and T. Meyer, Beitr. Plasmaphys. **23**, 9 (1983).
[6] Y. T. Lee and R. M. More, Phys. Fluids **27**, 1273 (1984).
[7] R. H. Williams and H. E. Dewitt, Phys. Fluids **12**, 2326 (1969).
[8] G. A. Rinker, Phys. Rev. B **31**, 4207 (1985).
[9] F. Perrot and M. W. C. Dharma-Wardana, Phys. Rev. A **36**, 238 (1987).
[10] J. P. Hansen, Phys. Rev. A **8**, 3096 (1973).
[11] W. L. Slattery, G. D. Doolen, and H. E. Dewitt, Phys. Rev. A **21**, 2087 (1980).
[12] I. M. Isakov, A. A. Likal'ter, B. N. Lomakin, A. D. Lopatin, and V. E. Fortov, Zh. Eksp. Teor. Fiz. **87**, 832 (1984) [Sov. Phys. JETP **60**, 473 (1984)].
[13] Y. V. Ivanov, V. B. Mintsev, V. E. Fortov, and A. N. Dremin, Zh. Eksp. Teor. Fiz. **71**, 216 (1971) [Sov. Phys. JETP **44**, 112 (1974)].
[14] A. Ng, D. Parfenink, P. Celliers, L. DaSilva, R. M. More, and Y. T. Lee, Phys. Rev. Lett. **57**, 1595 (1986).
[15] H. M. Milchberg, R. R. Freeman, S. C. Davey, and R. M. More, Phys. Rev. Lett. **61**, 2364 (1988).
[16] S. L. Gilbert, J. J. Bollinger, and D. J. Wineland, Phys. Rev. Lett. **60**, 2022 (1988).
[17] Y. Vitel, A. Mokhtari, and M. Skowronek, J. Phys. B **23**, 651 (1990).
[18] R. L. Shepherd, D. R. Kania, and L. A. Jones, Phys. Rev. Lett. **61**, 1278 (1988).
[19] A. N. Mostovych, K. J. Kearney, J. A. Stamper, and A. J. Schmitt, Phys. Rev. Lett. **66**, 612 (1991).
[20] V. E. Fortov and I. T. Iakubov, *Physics of Nonideal Plasma* (Hemisphere, New York, 1990).
[21] T. P. Hughes, *Plasmas and Laser Light* (Halstead, New York, 1975), p. 293.
[22] R. G. McQueen, S. P. Marsh, J. W. Taylor, J. N. Fritz, and W. J. Carter, in *High Velocity Impact Phenomena*, edited by R. Kinslow (Academic, New York, 1970), pp. 355–358.
[23] B. K. Y. Young, R. E. Stewart, J. G. Woodworth, and J. Bailey, Rev. Sci. Instrum. **57**, 2829 (1986).
[24] T. Oliphant, J. Comput. Phys. **38**, 406 (1980).
[25] J. F. Benage, Jr., E. G. Sherwood, and S. E. Linzey, Rev. Sci. Instrum. **63**, 5049 (1992).
[26] J. F. Benage, Jr. (unpublished).
[27] M. A. Bourham, O. E. Hankins, O. Auciello, J. M. Stock, B. W. Wehring, R. M. Mohanti, and J. G. Gilligan, IEEE Trans. Plasma Sci. **17**, 386 (1989).
[28] S. Ichimaru, in *Strongly Coupled Plasma Physics*, edited by H. M. Van Horn and S. Ichimaru (University of Rochester Press, Rochester, NY, 1993), pp. 31–40.

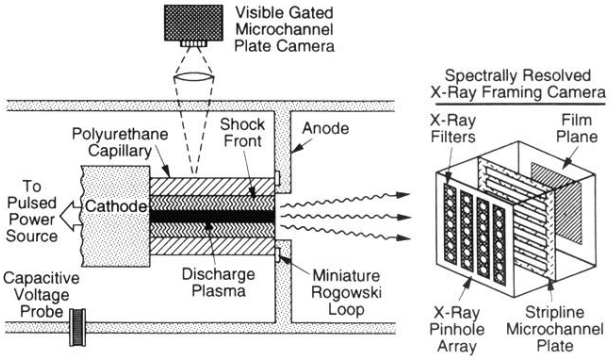

FIG. 1. A schematic of the experimental setup to measure the electrical resistivity in the plasma.

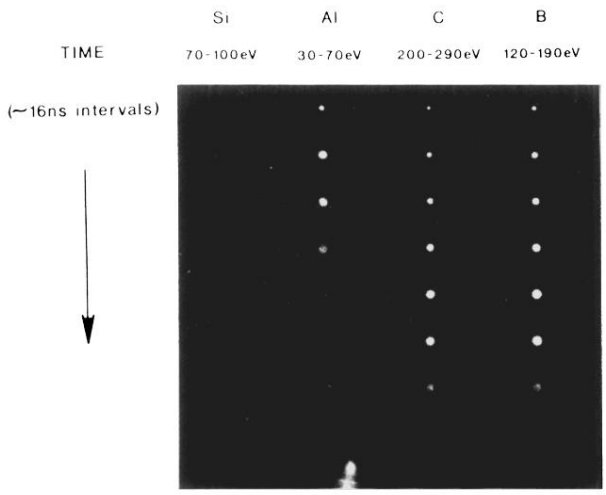

FIG. 6. Image of the end of the discharge using the pinhole x-ray framing camera. Each row is a single time and the time separation between each row is approximately 16 ns. Time goes from top to bottom. The columns each represent a different filter and from left to right these are 1.5 μm silicon, 0.65 μm aluminum, 2 μm paralyne-*N*, and 0.75 μm boron.